Supporting Information

Kmiec et al. 10.1073/pnas.1307637110

SI Experimental Procedures

Sequence Analysis. For visualization purposes, we constructed a phylogenetic tree of octapeptidyl aminopeptidase 1 (Oct1) and organellar oligopeptidase (OOP) homologs. A multiple sequence alignment was generated using MUSCLE (1), and the regions of poor alignment were removed using Gblocks (2) (maximum nonconserved positions = 8; minimum block length = 10). The tree was constructed using PhyML 3.0 (3) (Jones–Taylor–Thornton matrix) with 100 bootstrap replicates and was visualized using iTOL (http://itol.embl.de/).

Cloning and Constructs. The coding sequences of OOP and cytosolic oligopeptidase (CyOP) were cloned as follows. Briefly, total RNA was isolated from *Arabidopsis thaliana* leaves using the RNeasy Plant Kit (Qiagen), and total cDNA was synthesized using oligo (12-18)-dT primers and the ThermoScript reverse transcriptase System (Invitrogen). Full-length coding sequences were amplified using OOP-specific primers. To prepare constructs for GFP-based localization analysis, the sequences coding for the full-length OOP and CyOP were cloned to the pDONR221 vector and subsequently were subcloned to the pDEST/cGFP vector upstream of the GFP-coding cassette using Gateway technology (Invitrogen). The targeting signals of *Glycine max* alternative oxidase (AOX), Mitochondrial cherry (mit-cherry), *Pisum sativum* small subunit of ribulose-1,5-bisphosphate carboxylase/oxygenase, chloro-CFP (CD3-993), and the *Arabidopsis thaliana* actin-binding domain of the AtFIM1 protein (At4g26700) fused to RFP were used as a mitochondrial, plastid, and cytosolic markers, respectively (4–6). For the stable expression of FLAG-tagged peptidases, a sequence coding for a triple FLAG tag was added to the 5′ end of the OOP or CyOP coding sequence by PCR. The fusion constructs then were cloned to the pDONR221 vector and subsequently were subcloned to the pH2GW7 vector (VIB) using Gateway technology (Invitrogen). For overexpression in *Escherichia coli* an N-terminal deletion variant of OOP (Δ1–82) was cloned into the pGEX-6p-2 vector (GE Healthcare) downstream of the GST-coding cassette using BamHI and NotI restriction sites. Site-directed mutagenesis was performed using Quick Change II Site-Directed Mutagenesis Kit (Stratagene). All constructs were verified by sequencing.

Biolistic Transformation and Microscopy. Briefly, 5 μg of GFP and RFP plasmids were coprecipitated onto gold particles and were biolistically transformed into 4-d-old *Arabidopsis* cell suspensions using the PDS-1000/He biolistic transformation system (Bio-Rad). Transformants were incubated for 12 h at 22 °C in the dark. Fluorescence was visualized at 100× magnification using a BX61 Olympus microscope (Olympus) with the excitation wavelengths of 460/480 nm (GFP) and 535/555 nm (RFP) and emission wavelengths of 495–540 nm (GFP) and 570–625 nm (RFP). Images were captured using Cell^{R} imaging software (Olympus) as previously described (4).

Stable *A. thaliana* Transformation. *A. thaliana* plants were transformed using *Agrobacterium tumefaciens*-mediated infection according to the modified floral dip method (7). T1-generation transformants were selected on plates containing Murashige and Skoog medium with sucrose (3%) and Hygromycin B (15 μg /mL) (Sigma). Plants of the T3 generation were used for analysis.

Selection of Transfer DNA Insertion Knockout Lines and Phenotype Analysis. Transfer DNA (T-DNA) insertion *oop-1* (SALK_058439), *oop-2* (SALK_086727), and cyop-2 (SALK_086727.55.20) lines were purchased from the Salk Institute and were selected using recommended primers. Lack of expression was confirmed using RT-PCR. Briefly, total RNA was isolated from *A. thaliana* leaves using the RNeasy Plant Kit (Qiagen), and total cDNA was synthesized using random primers and the ThermoScript reverse transcriptase System (Invitrogen). Lack of protein expression was confirmed by immunodetection using anti-OOP antibodies. Growth progression was analyzed according to Boyes et al. (8). Gas exchange and chlorophyll fluorescence measurements were performed on 2-wk-old wild-type (Col-0), *oop-1*, and *oop-2* plants. Photosynthetic rate, transpiration rate, and water use efficiency were measured using the Whole Plant *Arabidopsis* chamber (LI-6400–17; LICOR Inc.) according to Msanne et al. (9) with modifications. Maximum fluorescence, effective photosystem II quantum yield, and electron transport rate were measured using the IMAGING-PAM M-series Chlorophyll Fluorescence System (Walz) according to Nilsson Cederholm et al. (10) with modifications ($n = 3$). The Turkey multiple comparisons of means (95% family-wise confidence level) were used to analyze results statistically ($P < 0.05$ was considered significant). The triple *oop-2 prep1 prep2*– and the double *oop-2 cyop-2*–knockout lines were obtained by genetic crossing. The purity of the lines was confirmed using PCR, RT-PCR, and immunoblotting.

In Vitro Translation. Precursor of OOP was synthesized in vitro using the TNT Coupled Reticulocyte Lysate System (Promega) in the presence of ^{35}S-labeled methionine (PerkinElmer). OOP translation products were separated by SDS/PAGE and detected by autoradiography.

Electrophoresis and Western Blotting. NuPAGE 4–12% Bis-Tris gels (Invitrogen) were used for $pF_1\beta_{2\text{-}54}$, $A\beta_{1\text{-}40}$, and general protein separation. Other peptides were analyzed on 16% Tris-Tricine SDS/PAGE (11). After electrophoresis proteins were transferred to a nitrocellulose membrane (GE Healthcare) and immunodecorated with antibodies. Detection was performed using an ECL system (GE Healthcare). The following antibodies were used in this study: anti-FLAG (F1804; Sigma), anti-AtPreP [recognizing residues 904–922 of AtPreP1 and the corresponding region of AtPreP2 (12)], anti-SHMT (serine hydroxymethyltransferase, AS05075; Agrisera), anti-Tim17.2 [Translocase of the inner mitochondrial membrane subunit 17.2 At2g37410 (13)], anti-PsbA (D1 protein, AS03084), anti-Tim9 [Translocase of the inner mitochondrial membrane subunit 9 At3g46560 (14)], anti-RbcL (Rubisco large subunit AS03037, Agrisera), anti-OOP (raised against overexpressed $OOP^{\Delta 1\text{–}82}$ to recognize both OOP and CyOP), and anti-UGPase (UDP-glucose pyrophosphorylase AS05086; Agrisera).

OOP-FLAG Immunoprecipitation. Samples of mitochondrial matrix (300 μg) and chloroplastic stroma (corresponding to 150 μg chlorophyll) isolated from *Arabidopsis* lines expressing OOP-FLAG were incubated with FLAG M2 affinity gel (Sigma) for 3 h at 4 °C. The M2 beads subsequently were washed three times with 50 mM Tris (pH 7.4) and 150 mM NaCl. Bound proteins were eluted with 2× SDS-sample buffer and analyzed by SDS/PAGE followed by Western blot.

Purification of Recombinant Wild-Type OOP and Variants. Plasmids pGEX6p2 encoding *A. thaliana* OOP lacking the putative targeting sequence (Δ1−82 aa) or presequence protease (PreP1) (12) were transformed into *E. coli* Rosetta 2 cells (Novagen). Cell cultures were grown in 1-L batches in Terrific Broth me-

dium (Formedium) containing 100 μg/μL ampicillin (Sigma) and 34 μg/μL chloramphenicol (Sigma) at 37 °C to OD_{600} ~0.6 and then were induced with 0.6 mM Isopropyl β-D-1-thiogalactopyranoside (Formedium) for 5 h (with the temperature adjusted to 23 °C). Cells then were harvested and frozen as pellets. The cell pellets were dissolved in glutathione (GSH)-binding buffer [140 mM NaCl, 2.7 mM KCl, 10 mM Na_2HPO_4, 1.8 mM KH_2PO_4 (pH 7.3), 2.5 mM DTT, 10 mM $MgCl_2$, 1 μM Zn acetate] containing 1 mg /mL lysozyme (Sigma) and 10 μg /mL DNaseI (Sigma) and then were incubated for 1 h at 4 °C for cell lysis. The cell extract was centrifuged at 4,000 × *g* to remove unbroken cells, and the supernatant was further centrifuged at 100,000 × *g*. The soluble fraction was incubated with Glutathione Sepharose (GE Healthcare) for 4 h and then was washed four times with GSH-binding buffer and twice with cleavage buffer [50 mM Tris·HCl (pH 7.5), 150 mM NaCl, 2.5 mM DTT). Twenty units of HRV3C protease (MoBiTec) were applied, and the protein was eluted after overnight incubation at 4 °C. The resulting sample was then applied to a Superdex 200 10/300 GL size-exclusion column equilibrated in 10 mM Hepes (pH 7.4), 50 mM NaCl, and 1 mM DTT.

Crystallization and Structure Determination. Crystals were grown by vapor diffusion in a sitting-drop experiment. OOP^{E572Q} or wild-type OOP (10 mg/mL) was mixed in a 1:1 ratio with reservoir solution [18–22% poly(ethylene glycol) methyl ether 5000, 0.1 M Bis-tris-propane (pH 6.5), and 0.2 M Na-malonate]. Well-diffracting crystals appeared after 3–5 d incubation at 18 °C. Crystals were soaked in reservoir solution supplemented with 20% glycerol before being flash-cooled in liquid nitrogen. Data were collected at the beamlines 14.1 at the Berliner Elektronenspeicherring-Gesellschaft für Synchrotronstrahlung (Berlin) and I911-3 at the MAX-Laboratory (Lund) and at PX1, Swiss Light Source (Villigen) (Table S1). Data processing and reduction were carried out using XDS (15) and programs from the CCP4 suite (16). The phase problem was solved via molecular replacement using the *E. coli* dipeptidyl carboxypeptidase (Protein Data Bank code: 1Y79) as a search model. An initial model containing *ca*. 95% of the residues could be built using ARP/wARP (17). A few cycles of refinement using Refmac5 (18), interspersed with manual building in Coot (19), were needed to complete the models. Water molecules were placed automatically in F_O-F_C Fourier difference maps at 3σ cutoff levels and subsequently were validated to ensure their correct placement. Translation/Libration/Screw parameters were used during the last steps of refinement (20). The final model contains residues 92–785; the remaining 14 N-terminal and six C-terminal residues were flexible and thus were not visible in the electron density map. Correct placement of the catalytic Zn atom was validated by anomalous data collected at the zinc edge on the OOP^{E572Q} crystals. All structure figures were prepared using PyMOL (www.pymol.org). The cavity analysis and volume calculation were performed with data from Caver (21).

Peptide Synthesis. Peptides ($pF_1\beta$ 4-15, $pF_1\beta$ 43-53, pL29, pACD1, tpACS 1-11, and tpACS 1-19) were synthesized on Rink-amide Chemmatrix resin (PCAS BioMatrix) using fluorenylmethyloxycarbonyl solid-phase peptide synthesis on a SYRO II peptide synthesizer (MultiSynTech). Cl-HOBT and HTCU were used as coupling reagents. The crude peptide was cleaved for 3 h in a mixture of 95% trifluoroacetic acid, 2.5% water, and 2.5% triisopropylsilane, precipitated in cold diethyl ether and purified by reversed-phase HPLC on a BioBasic C-8 column (Thermo Scientific) using a gradient of water/acetonitrile (ACN) with the addition of 0.1% trifluoroacetic acid. The purified peptide was lyophilized and analyzed by matrix-assisted laser desorption ionization time-of-flight MS on a Voyager-DE STR (Applied Biosystems) using α-Cyano-4-hydroxycinnamic acid as matrix.

Sample Preparation and MS Analysis. Peptides $pF_1\beta$ 4-15, $pF_1\beta$ 43-53, pL29, pACD1, Cyt1p, pCox4, pThrRS 1-19, tpACS 1-11, tpACS 1-19, tpACS 1-26, and octMdh1, octSdh1, and SytII (4 μg each) were mixed with 1 μg of OOP or AtPreP1 for 2 h at 30 °C. After the enzymatic assay, 3 μL (corresponding to 600 ng of total peptide amount) from each sample was acidified by addition of 15 μL of 10% formic acid (FA) solution. The acidified solution of each sample then was run in analytical triplicates. In each liquid chromatography (LC)-MS run, the LC auto sampler (HPLC 1200 system; Agilent Technologies) injected 3 μL into a C18 guard desalting column (Zorbax 300SB-C18; Agilent). We then used a 15-cm-long C18 picofrit column (Nikkyo Technos Co.) installed on to the nano electrospray ionization source. Solvent A was 97% water, 3% ACN, 0.1% FA, and solvent B was 5% water, 95% ACN, 0.1% FA. At a constant flow of 0.4 $\mu L \cdot min^{-1}$, the linear gradient went from 2 to 40% B in 15 min, followed by a steep increase to 100% B in 5 min. Online LC-MS was performed using a hybrid Q-Exactive mass spectrometer (Thermo Scientific). Fourier transform MS master scans with 70,000 resolution (and mass range 300–1700 *m/z*) were followed by data-dependent MS/MS (17,500 resolution) on the top five ions using higher energy collision dissociation at 30% normalized collision energy. Precursors were isolated with a 2-*m/z* window. Automatic gain control targets were 1e6 for MS1 and 1e5 for MS2. Maximum injection times were 100 ms for MS1 and 500 ms for MS2. The entire duty cycle lasted ~2.5 s. Dynamic exclusion was used with a 60-s duration. Precursors with unassigned charge state or charge state 1 were excluded. An underfill ratio of 1% was used. All MS/MS spectra were searched by Sequest under the software platform Proteome Discoverer (v1.3.0.339; Thermo Scientific) against a FASTA file containing all the sequences of the peptides used as substrates in the enzymatic assay. Precursor mass tolerance of 10 ppm and product mass tolerance of 0.02 Da were used. Oxidation of methionine and amidation of the C terminus were used as variable modifications. Precursor peak areas were quantified using the "precursor ions area detector" module of Proteome Discoverer (Dataset S1). Only peaks with an area of at least 5% of the intact peptide peak were used in the interpretation of the cleavage pattern. The selected peaks are highlighted in Dataset S1. The raw mass spectrometry data have been deposited in the ProteomeXchange Consortium (http://proteomecentral.proteomexchange.org/cgi/GetDataset) via the PRIDE partner repository with the dataset identifier PXD000444. Endogenous peptides bound to OOP were released by denaturation of 15 μg of OOP (resuspended in 10 mM Hepes, pH 7.0) using 0.4% SDS at 37 °C for 15 min. Endogenous peptides were purified using a ZipTip μ-C18 (Millipore) following the manufacturer's instructions. After drying in a SpeedVac, peptides were redissolved in 20 μL of solvent A, and 1 μL was injected and run in LC-MS as described above.

1. Edgar RC (2004) MUSCLE: Multiple sequence alignment with high accuracy and high throughput. *Nucleic Acids Res* 32(5):1792–1797.
2. Talavera G, Castresana J (2007) Improvement of phylogenies after removing divergent and ambiguously aligned blocks from protein sequence alignments. *Syst Biol* 56(4):564–577.
3. Guindon S, et al. (2010) New algorithms and methods to estimate maximum-likelihood phylogenies: Assessing the performance of PhyML 3.0. *Syst Biol* 59(3):307–321.
4. Carrie C, et al. (2009) Approaches to defining dual-targeted proteins in Arabidopsis. *Plant J* 57(6):1128–1139.
5. Carrie C, Murcha MW, Millar AH, Smith SM, Whelan J (2007) Nine 3-ketoacyl-CoA thiolases (KATs) and acetoacetyl-CoA thiolases (ACATs) encoded by five genes in Arabidopsis thaliana are targeted either to peroxisomes or cytosol but not to mitochondria. *Plant Mol Biol* 63(1):97–108.
6. Ng S, et al. (2013) A membrane-bound NAC transcription factor, ANAC017, controls mitochondrial retrograde signaling in Arabidopsis. *Plant Cell*, in press.
7. Martinez-Trujillo M, Limones-Briones V, Cabrera-Ponce J, Herrera-Estrella L (2004) Improving transformation efficiency of Arabidopsis thaliana by modifying the floral Dip. *Plant Mol Biol Rep* 22(1):63–70.

8. Boyes DC, et al. (2001) Growth stage-based phenotypic analysis of Arabidopsis: A model for high throughput functional genomics in plants. *Plant Cell* 13(7):1499–1510.
9. Msanne J, Lin J, Stone JM, Awada T (2011) Characterization of abiotic stress-responsive Arabidopsis thaliana RD29A and RD29B genes and evaluation of transgenes. *Planta* 234(1):97–107.
10. Nilsson Cederholm S, Bäckman HG, Pesaresi P, Leister D, Glaser E (2009) Deletion of an organellar peptidasome PreP affects early development in Arabidopsis thaliana. *Plant Mol Biol* 71(4-5):497–508.
11. Schägger H (2006) Tricine-SDS-PAGE. *Nat Protoc* 1(1):16–22.
12. Moberg P, et al. (2003) Characterization of a novel zinc metalloprotease involved in degrading targeting peptides in mitochondria and chloroplasts. *Plant J* 36(5):616–628.
13. Murcha MW, Elhafez D, Millar AH, Whelan J (2005) The C-terminal region of TIM17 links the outer and inner mitochondrial membranes in Arabidopsis and is essential for protein import. *J Biol Chem* 280(16):16476–16483.
14. Wang Y, et al. (2012) Dual location of the mitochondrial preprotein transporters B14.7 and Tim23-2 in complex I and the TIM17:23 complex in Arabidopsis links mitochondrial activity and biogenesis. *Plant Cell* 24(6):2675–2695.
15. Kabsch W (2010) XDS. *Acta Crystallogr D Biol Crystallogr* 66(Pt 2):125–132.
16. Anonymous; Collaborative Computational Project, Number 4 (1994) The CCP4 suite: Programs for protein crystallography. *Acta Crystallogr D Biol Crystallogr* 50(Pt 5):760–763.
17. Cohen SX, et al. (2008) ARP/wARP and molecular replacement: The next generation. *Acta Crystallogr D Biol Crystallogr* 64(Pt 1):49–60.
18. Murshudov GN, Vagin AA, Dodson EJ (1997) Refinement of macromolecular structures by the maximum-likelihood method. *Acta Crystallogr D Biol Crystallogr* 53(Pt 3):240–255.
19. Emsley P, Cowtan K (2004) Coot: Model-building tools for molecular graphics. Acta Crystallogr D Biol Crystallogr 60(Pt 12 Pt 1):2126–2132.
20. Winn MD, Isupov MN, Murshudov GN (2001) Use of TLS parameters to model anisotropic displacements in macromolecular refinement. *Acta Crystallogr D Biol Crystallogr* 57(Pt 1):122–133.
21. Chovancova E, et al. (2012) CAVER 3.0: A tool for the analysis of transport pathways in dynamic protein structures. *PLOS Comput Biol* 8(10):e1002708.

A

Fig. S1. (Continued)

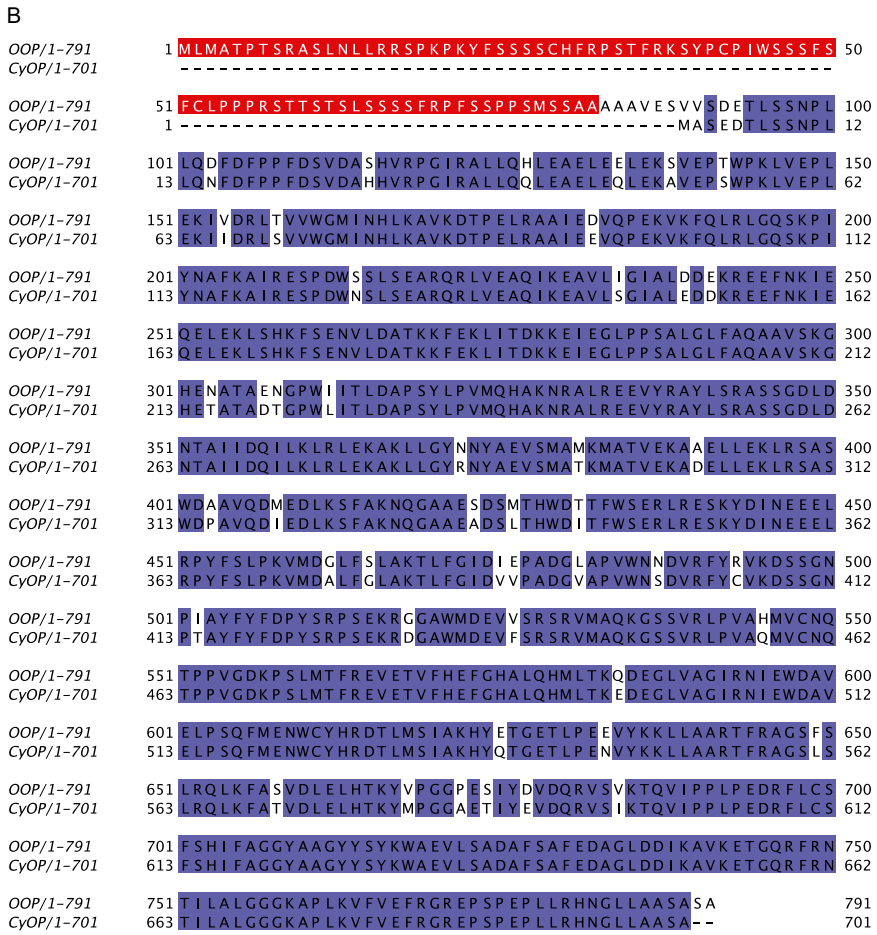

Fig. S1. Protein sequence alignment of M3A peptidase homologs constructed using MUSCLE. (*A*) Multiple sequence alignment of M3A homologs from several organisms: *A. thaliana* (At1g67690, At5g65620, At5g10540, At5g51540); *Saccharomyces cerevisiae* (ScOct1, ScPRD1); *Homo sapiens* (HsOct1, HsNeurolysin); *Rattus norvegicus* (RnOct1); and *E. coli* (EcOpdA). (*B*) Alignment of *A. thaliana* at5g65620/OOP and at5g10540/CyOP. The targeting peptide predicted by TargetP (www.cbs.dtu.dk/services/TargetP/) is shown in red.

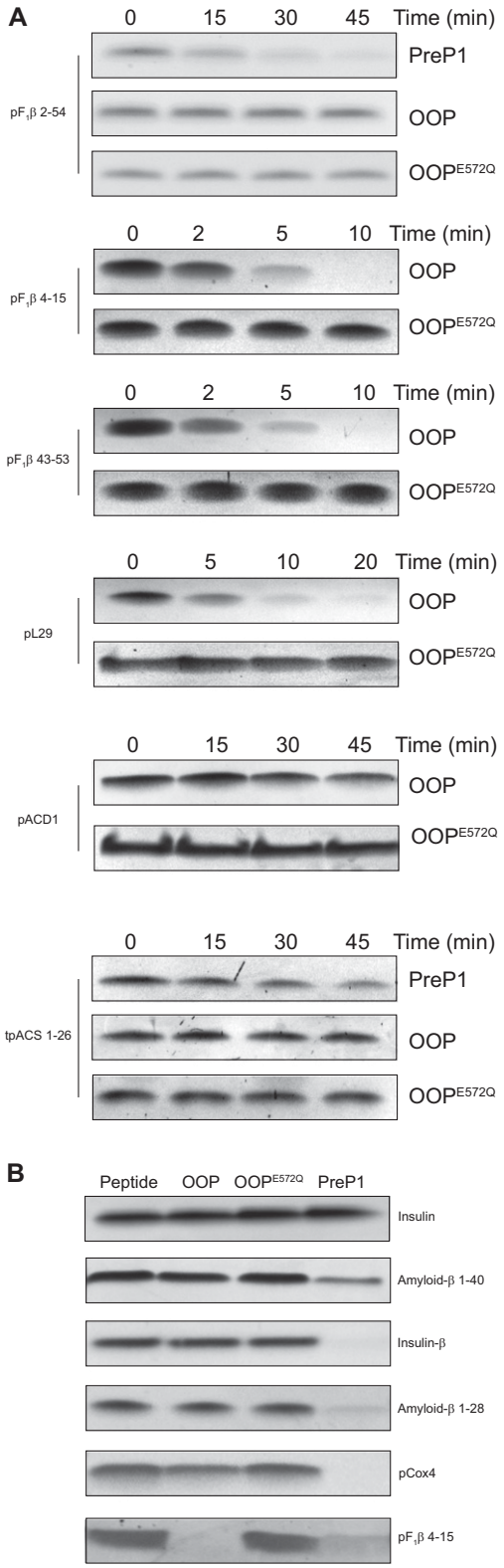

Fig. S2. Peptide degradation by OOP. (*A*) Degradation of $pF_1\beta$ derivatives, pL29, pACD1, and tpACS 1-26 peptides analyzed by SDS/PAGE (performed in duplicate in each case; shown are representative results). The intensity of the bands was quantified using MultiGauge software; results are summarized in Fig. 3. Reactions were run in duplicate for the indicated time at 30 °C. (*B*) Degradation of peptides by OOP, with PreP1 and OOP^{E572Q} used as controls. Reactions were run for 1 h at 30 °C.

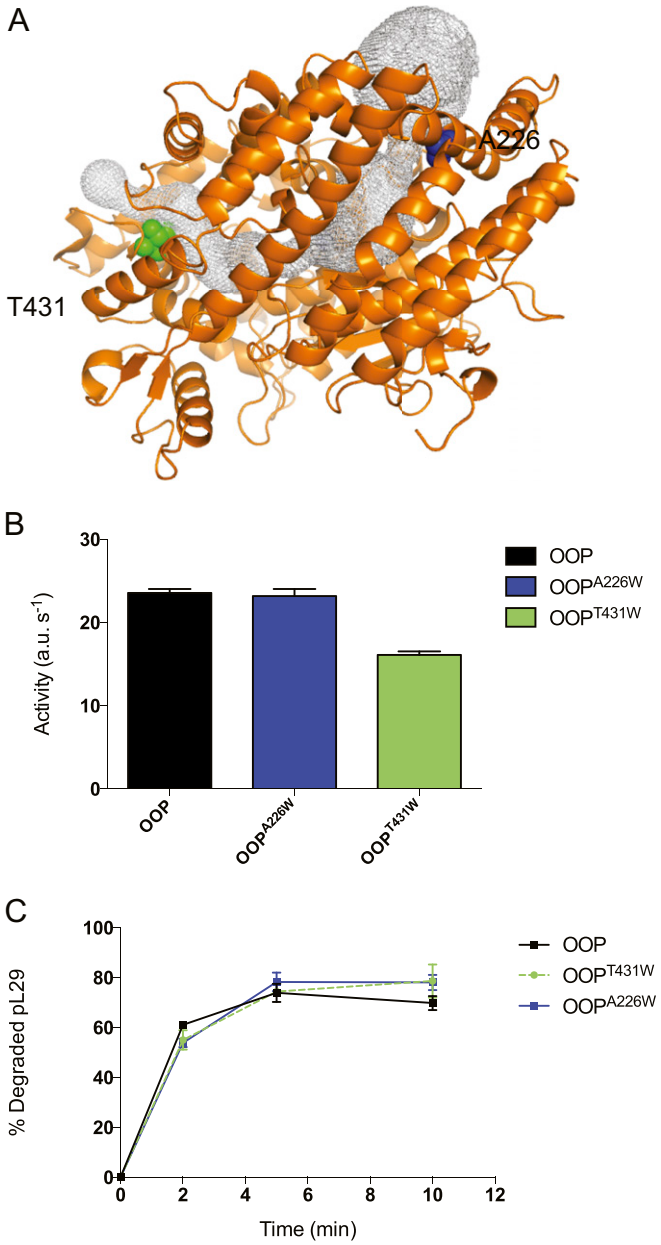

Fig. S3. Analysis of OOP variants that obstruct the exit points in the internal cavity. (*A*) Ribbon diagram highlighting the location of residues A226 and T431 within the OOP structure. (*B* and *C*) Graphs showing the activity of the variants OOP^{A226W} and OOP^{T431W} in the degradation of the bradykinin-derived Substrate V (*B*) and the presequence pL29 (*C*).

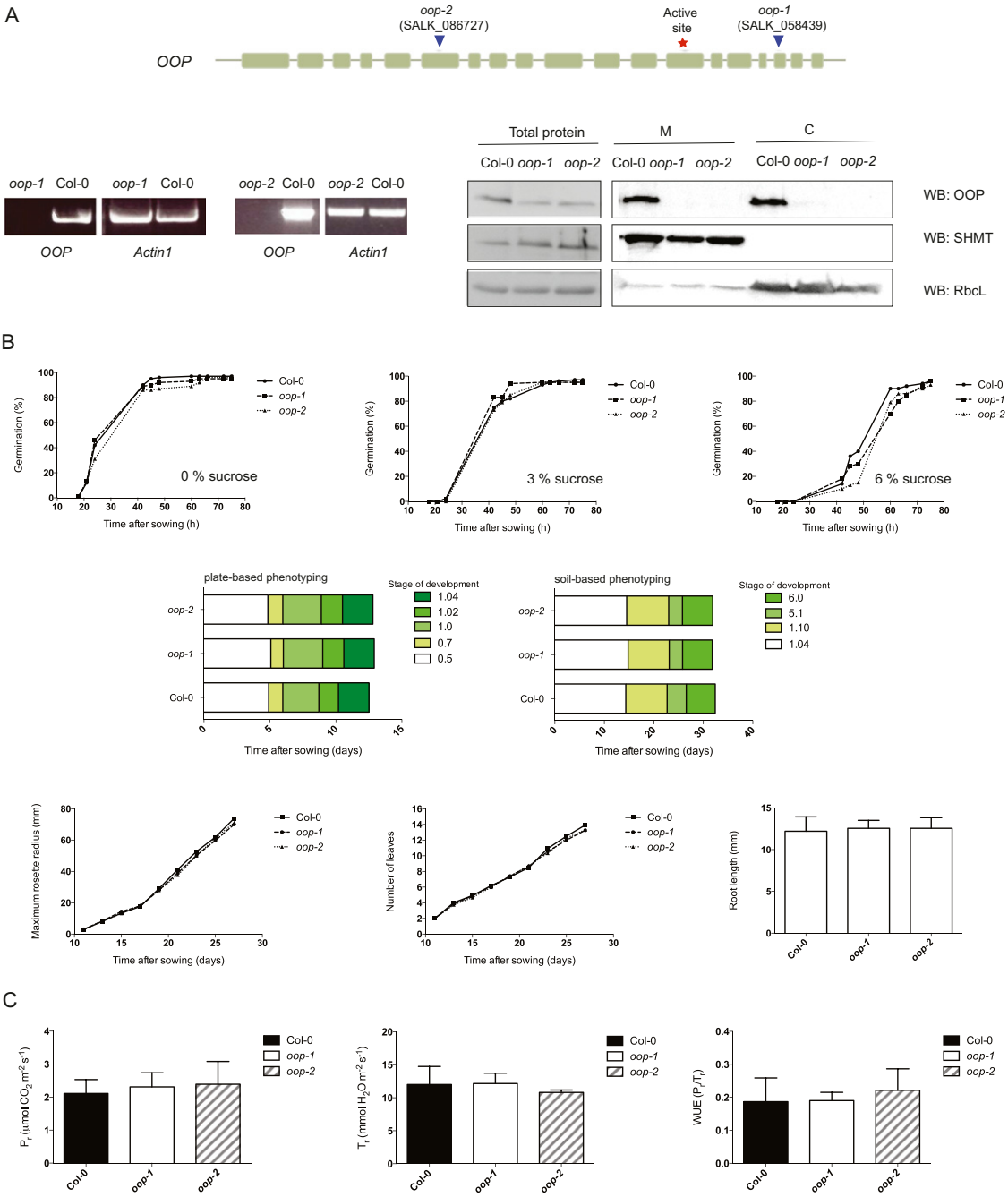

Genotype	Fm	Y(II)	ETR
Col-0	0.182 ± 0.016	0.957 ± 0.0044	43.07 ± 0.2
oop-1	0.157 ± 0.011	0.953 ± 0.0032	42.90 ± 0.15
oop-2	0.171 ± 0.011	0.966 ± 0.0027	43.47 ± 0.12

Fig. S4. Selection of *A. thaliana oop*-knockout plants. Two independent T-DNA–insertion *oop*-knockout lines were selected: *oop-1* (SALK_058439) and *oop-2* (SALK_086727). (*A*) (*Upper*) *OOP* gene structure with exons and introns represented as green boxes or a green line, respectively. The positions of the insertions, verified by sequencing, are indicated by blue arrowheads; the position of the active site is marked with a red star. (*Lower*) *oop-1* and *oop-2* plants do not express *OOP*. Results of RT-PCR obtained using total RNA isolated from *oop*-knockout plants (*oop-1* and *oop-2*) and wild-type (Col-0) plants. Amplification of the transcript for the *Actin 1* gene (At2g37620) was used as control. *oop-1* and *oop-2* plants do not produce OOP, as was confirmed by RT-PCR and immunological detection of OOP in total protein extract, mitochondria, and chloroplasts isolated from wild-type (Col-0), *oop-1*, and *oop-2* plants. OOP antibodies recognize both OOP and CyOP; therefore CyOP is detected in the total extract isolated from *oop*-knockout plants. However, because of the cytoplasmic localization of CyOP, only OOP is detected in isolated organelles. Lack of the signal in the organelles isolated from *oop* plants confirms that both *oop-1* and *oop-2* lines are knockout mutants. To verify equal loading and purity of isolated organelles, we used antibodies raised against serine hydroxymethyltransferase (SHMT); a mitochondrial marker) and RbcL, a chloroplastic marker. (*B*) Phenotypic analysis of wild-type, *oop-1*–, and *oop-2*–knockout plants. (*Top*) Comparison of germination rates. Plants were grown on plates containing Murashige and Skoog medium plus 0, 3, or 6% sucrose ($n = 100$). (*Middle*) Plate- and soil-based

Legend continued on following page

growth progression analysis. During the plate-based analysis, plants were grown on plates containing Murashige and Skoog medium containing 3% sucrose ($n = 15$). The following developmental stages were analyzed: 0.5 (first radicle emerged), 0.7 (cotyledon visible), 1.0 (cotyledon fully opened), 1.02 (two rosette leaves >1 mm), 1.04 (four rosette leaves >1 mm), 1.10 (10 rosette leaves >1 mm), 5.1 (first flower bud visible), and 6.0 (first flower open). (*Bottom*) Comparison of the maximum rosette radius, number of leaves (soil-based analysis), and root length (plate-based analysis at stage 1.02) ($n = 15$). (*C*) Gas exchange and chlorophyll fluorescence parameters analysis. (*Upper*) Gas exchange parameters: photosynthetic rate (P_r), transpiration rate (T_r), and water use efficiency (WUE) for 2-wk-old plants ($n = 3$). (*Lower*) Chlorophyll fluorescence parameters: maximum fluorescence yield (Fm), effective PSII quantum yield [Y(II)], and electron transport rate (ETR) for 2-wk-old plants ($n = 3$).

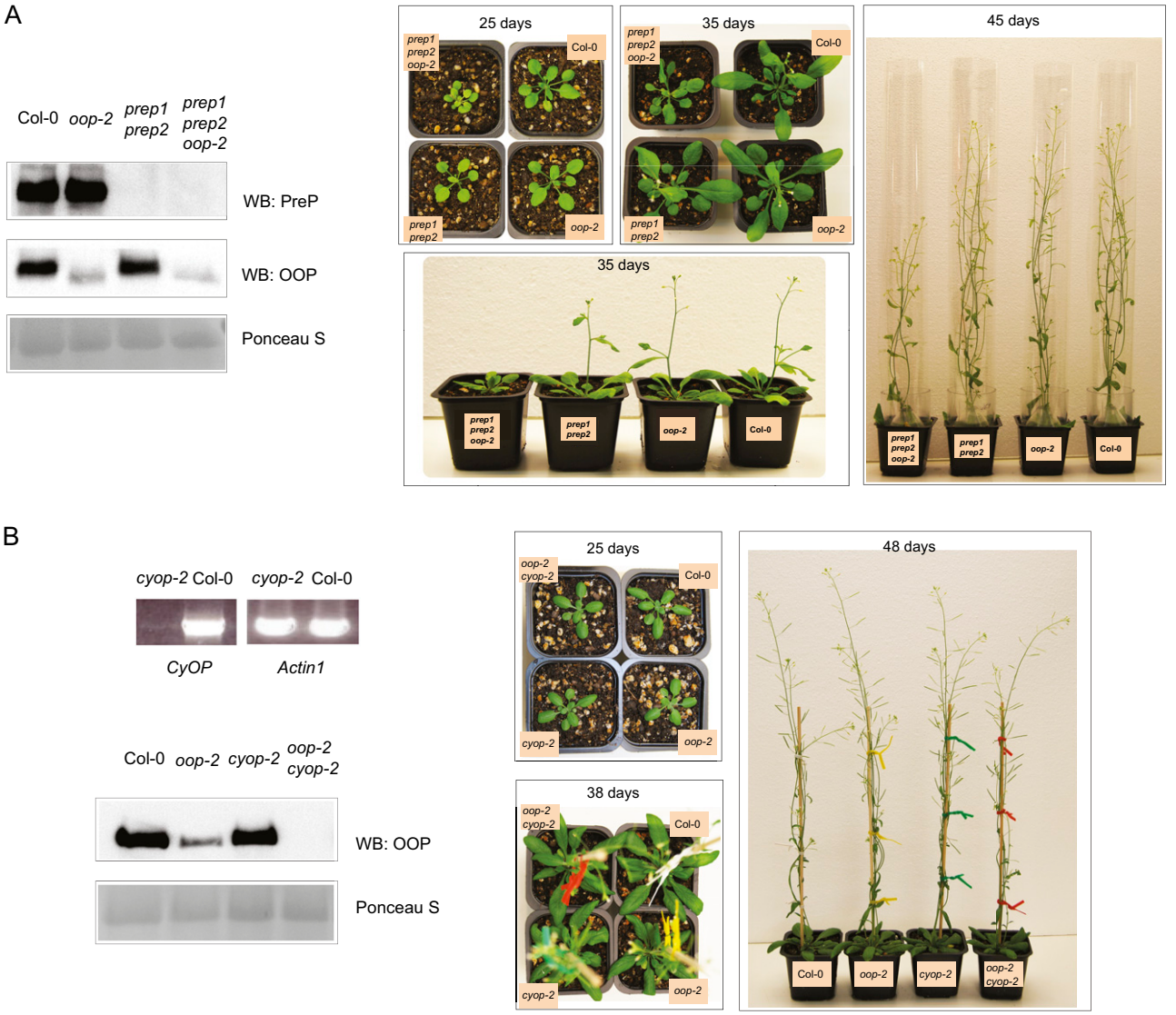

Fig. S5. Analysis of OOP interaction with AtPreP and CyOP (*A*) Analysis of *prep1 prep2 oop* triple-knockout plants. Lack of AtPreP and OOP expression was confirmed by immunodetection using total protein extract isolated from leaves of wild-type (Col-0), *oop-2*, *prep1 prep2* double-knockout, and *prep1 prep2 oop* triple-knockout plants. (*B*) Analysis of *oop cyop* double-knockout plants. Lack of CyOP expression in the *cyop-2* line (SALK_086727.55.20) was determined by RT-PCR. The position of the T-DNA insertion (exon 5) was verified by sequencing. Amplification of the transcript for *Actin 1* gene (At2g37620) was used as control. Lack of expression of OOP and CyOP in the *oop cyp* double knockout was confirmed by immunodetection using total protein extract isolated from leaves of wild-type (Col-0), *oop-2*, *cyop-2*, and *cyop oop* double-knockout plants. Anti-OOP antibodies recognize both OOP and CyOP; therefore signal is detected in the single knockouts. (*C*) FLAG immunoprecipitation from samples of mitochondrial matrix and chloroplastic stroma isolated from *Arabidopsis* lines expressing OOP-FLAG. Matrix and stromal samples were incubated with M2 affinity beads. Both the proteins bound to the beads, and the supernatant fractions were analyzed by Western blot with antibodies against FLAG, PreP, RbcL (stromal marker), and SHMT (matrix marker).

Table S1. Data collection and refinement statistics

	OOP^{E572Q}	*OOP wild-type*
Data collection		
Wavelength, Å	1.281	1.0
Space group	$P2_12_12_1$	$P2_12_12_1$
Cell dimensions		
a, b, c; Å	71.5, 100.8, 132.5	71.8, 101.3, 132.9
α, β, γ; °	90, 90, 90	90, 90, 90
Resolution, Å	29.1–1.8	47.3–1.9
R_{sym}, %	5.8 (50.2)	4.2 (43.5)
I/σ, I	17.0 (3.0)	12.5 (2.2)
Completeness, %	99.5 (98.1)	99.2 (99.2)
Redundancy	3.8 (3.6)	3.3 (3.1)
Refinement		
Resolution	29.1–1.8	47.3–1.9
No. unique reflections	84,471	72,514
R_{work}/R_{free}, %	17.9/19.9	19.1/21.8
No. atoms		
Protein	5,642	5,642
Ligand	20	—
Water	681	376
B-factors		
Protein	26.6	36.2
Ligand	47.7	—
Water	37.5	43.8
Rmsd		
Bond lengths, Å	0.007	0.011
Bond angles, °	1.10	1.37

Values in parenthesis are for the highest-resolution shell.

Other Supporting Information Files

Dataset S1 (XLSX)
Dataset S2 (XLSX)